MULTIRESOLUTION SEGMENTATION FOR EXTRACTING PLASTIC GREENHOUSES FROM DEIMOS-2 IMAGERY

Rafael Jiménez-Lao [1], Manuel A. Aguilar [1,*], Claudio Ladisa [2], Fernando J. Aguilar [1], Abderrahim Nemmaoui [1]

[1] University of Almería. Department of Engineering and Research Centre CIAIMBITAL. Almería 04120, Spain (rjl020, maguilar, faguilar, an932)@ual.es
[2] Politecnico di Bari. DICATECh, Via Orabona 4, Bari 70125, Italy (ladisaclaudio@gmail.com)

Commission II, WG II/6

KEY WORDS: Plastic Covered Greenhouse, Multiresolution Segmentation, VHR Satellite, OBIA, Deimos-2.

ABSTRACT:

Accurate greenhouse mapping can support environment monitoring and resource management. In an object-based image analysis (OBIA) approach focused on plastic covered greenhouses (PCG) classification, the segmentation is a crucial step for the goodness of the final results. Multiresolution segmentation (MRS) is one of the most used algorithms in OBIA approaches, being greatly enabled by the advent of the commercial software eCognition. Therefore, in addition to the segmentation algorithm used, it is very important to count on tools to assess the quality of segmentation results from digital images in order to obtain the most similar segments to the real PCG objects. In this work, several factors affecting MRS such as the type of input image and the best MRS parameters (i.e., scale, compactness and shape), have been analysed. In this regard, more than 2800 segmentations focused on PCG land cover were conducted from four pre-processed Deimos-2 very high-resolution (VHR) satellite orthoimages taken in the Southeast of Spain (Almería). Specifically, one multispectral and one pansharpened Deimos-2 orthoimages, both with and without atmospheric correction were tested in this work. The free access AssesSeg command line tool, based on a modified version of the supervised discrepancy measure named Euclidean Distance 2 (ED2), was used to determine the best MRS parameters for all the VHR satellite images. According to both the supervised discrepancy measure ED2 and visual perception, the best segmentation on PCG was obtained over the atmospherically corrected pansharpened Deimos-2 orthoimage, achieving very good results.

1. INTRODUCTION

The latest breed of very high resolution (VHR) commercial satellites successfully launched over the last decade (e.g., Pléiades-HR 1A (from 2011, 0.7 m GSD), Kompsat-3 (from 2012, 0.70 m GSD), Pléiades-HR 1B (from 2012, 0.7 m GSD), Skysat (from 2013, 0.90 m GSD), Kazeosat-1 (from 2014, 1 m GSD), Deimos-2 (from 2014, 1 m GSD), WorldView-3 (from 2014, 0.31 m GSD), Kompsat-3A (from 2015, 0.55 m GSD), TripleSat (from 2015, 1 m GSD), Teleos-1 (from 2015, 1 m GSD), WorldView-4 (from 2016 to 2019, 0.25 m GSD), Vision-1 (from 2018, 0.9 m GSD), SuperView1A/1B (from 2018, 0.5 m GSD), Jilin-1 (from 2019, 1 m)) has marked a turning point in the field of remote sensing. Since the advent of VHR satellite images, they have been increasingly used in remote sensing applications. Moreover, most of the Land Use/Land Cover (LULC) remote sensing classification research works from this type of satellite images were conducted using object-based image analysis (OBIA) techniques (Carleer and Wolff, 2006; Pu, Landry and Yu, 2011; Stumpf and Kerle, 2011; Pu and Landry, 2012; Aguilar et al., 2013; Fernández et al., 2014; Pacifici et al., 2014; Heenkenda et al., 2015; Hossain and Chen, 2019; Kotaridis and Lazaridou, 2021).

An object or segment is the basic element for an OBIA classification. So, the first step of the OBIA approach is the segmentation, where similar neighbouring pixels representing the same thing (e.g., house, tree, greenhouse,…) are grouped into segments or objects. Then the image classification is performed on objects rather than pixels by using meaningful features related to spectral values (e.g., mean spectral values, spectral indices), object shape, texture and context information associated with each object, so having a great potential to efficiently handle more difficult image analysis tasks (Marpu et al., 2010; Blaschke et al., 2014), especially when working on VHR satellite images. The quality of the segmentation significantly influences the final classification accuracy (Blaschke et al., 2014; Witharana and Civco, 2014) since it is in this first stage in which the image objects are generated, thus determining their corresponding attributes.

Ideally, one segment should represent one object of interest, and the segment boundary should match perfectly with the real object shape. However, in practice, an object of interest is represented by more than one segment (over-segmentation) or one segment represents two or more real objects belonging to different classes (under-segmentation) (Mesner and Oštir, 2014). Another problem with the segmentation process is that the boundaries of the segments do not match the boundaries of the object of interest. Therefore, it is very important to pay special attention to the segmentation step when using an OBIA approach, assessing its goodness before proceeding to the final classification stage. A comprehensive overview of existing segmentation-evaluation methods as well as their advantages and disadvantages was given by Zhang et al. (2008), and more recently by Johnson and Ma (2020) and Jozdani and Chen (2020). A few works have been published dealing with image segmentation based on Sentinel-1 and Sentinel-2 data (e.g., Tetteh et al., 2021; Petrushevskyet al., 2022). Novelli et al. (2017) published a freely available command line tool named AssesSeg to assess the quality of segmentations derived from satellite images in a supervised way (AssesSeg tool is available in: https://w3.ual.es/Proyectos/GreenhouseSat/index_archivos/links.htm). AssesSeg was based on a modified version of the Euclidean Distance 2 (ED2) discrepancy measure originally proposed by Liu et al. (2012). AssesSeg tool was already successfully tested to estimate the best MRS parameters from

* Corresponding author

Sentinel-2, Landsat 8 and WorldView-2 imagery for mapping PCG (Novelli et al., 2016, 2017).

Accurate PCG mapping using remote sensing methods presents a special challenge due to the unique characteristics of plastic coverings, such as different materials and spectral signatures, types of crops and phenological status, age, state of conservation and cleanliness of the plastic film, and local agricultural practice (Jiménez-Lao et al., 2020).
The OBIA approach focused on mapping PCG is much more recent than pixel-based analysis. Tarantino and Figorito (2012) published the first work based on OBIA to map plastic covered vineyards from true colour (RGB) aerial data in Bari, Southern Italy. Aguilar et al. (2014) also applied OBIA techniques on WorldView-2 and GeoEye-1 stereo imagery using Nearest Neighbour (NN) and SVM classifiers to achieve an overall accuracy of around 90% on PCG. Novelli et al. (2016) carried out the first work based on Sentinel-2 MSI and Landsat 8 OLI images to map PCG from adopting an OBIA approach and Random Forest (RF) classifier. All these OBIA researches used the MRS algorithm implemented in eCognition software.

The main objective of this communication is to assess the segmentation process in a PCG area over VHR satellite imagery with different pre-processing steps, and using MRS algorithm. Concretely, one multispectral (MS) and one pansharpened (PANSH) Deimos-2 orthoimages, both with and without atmospheric correction, were the four image sources on which numerous segmentations were obtained and evaluated using AssesSeg.

2. STUDY SITE AND DATASETS

2.1 Study Site

This investigation was conducted in an area with a great concentration of PCG located in Almería, Southeast of Spain. The study area comprised a rectangle area of about 5,000 ha centred on the WGS84 geographic coordinates of 36.7824°N and 2.6867°W (Fig. 1 and Fig. 2).

Figure 1. Location of the study area.

2.2 WorldView-3 RGB orhoimage

WorldView-3 (WV3) is a VHR satellite successfully launched on August 13, 2014. This sensor provides optical images with 0.31 m and 1.24 m ground sample distance (GSD) at nadir in panchromatic (PAN) and MS mode, respectively. The MS image is composed of 8 bands such as coastal (C, 400–450 nm), blue (B, 450–510 nm), green (G, 510–580 nm), yellow (Y, 585–625 nm), red (R, 630–690 nm), red edge (RE, 705–745 nm), near infrared-1 (NIR1, 770–895 nm) and near infrared-2 (NIR2, 860–1040 nm). A single WV3 bundle image in Ortho Ready Standard Level-2A (ORS2A) format was acquired on June 11, 2020. The off-nadir angle of the WV3 image was 27.6 degrees, with collected pixel sizes of 0.38 m in PAN and 1.52 m in MS mode. The final product presented GSD values of 0.3 m for PAN and 1.2 m for MS.

From the PAN and MS WV3 images, a PANSH image with 0.3 m GSD and three bands (RGB) was attained by means of the PANSHARP module included in Geomatica v. 2018 (PCI Geomatics, Richmond Hill, ON, Canada).

For the WV3 PANSH image, very accurate coordinates of seven ground control points (GCPs) measured by differential global positioning systems (DGPS), were used to compute the sensor model based on rational functions refined by a zero-order transformation in the image space (RPC0).

A medium resolution 10 m grid spacing DEM with a vertical accuracy of 1.34 m (root mean square error (RMSE)), provided by the Andalusian Government, was used to carry out the orthorectification process. A PANSH RGB WV3 orthoimage with 0.3 m GSD was generated using Geomatica v. 2018. The WV3 PANSH RGB orthoimage was used to manually digitalised the 400 reference PCG (see section 2.4)

2.3 Deimos-2 Data and Pre-processing

Deimos-2 is a VHR optical satellite fully owned and operated by Deimos Imaging, an UrtheCast company. It was launched in June 2014 and operates from a Sun-synchronous orbit at a mean altitude of 620 km. It can provide 1 m PAN and 4 m MS images with four bands (R, G, B, NIR) within a swath of 12 km at nadir. A single Deimos-2 bundle image (PAN+MS) level 1B (L1B), was acquired on July 30, 2019, covering the whole study area. L1B product involves calibration and radiometric correction, but it does not include resampling to a map grid. This basic product include the RPCs (sensor camera model) and the metadata with gain and bias values for each band. The collected Deimos-2 image presented an off-nadir angle of 35.2 degrees.

Again, the photogrammetric module of Geomatica v. 2018, called OrthoEngine, was used to perform both the orientation and the orthorectification phases. Also, a PANSH Deimos-2 image with 1 m GSD and four bands (R, G, B, NIR) was achieved from fusing PAN and MS images by means of the PANSHARP module included in Geomatica v. 2018.

According to Aguilar et al. (2020), a sensor model based on rational functions refined by a first-order transformation in the image space (RPC1) supported on 12 GCPs was used to carry out the orientation phase of the Deimos-2 optical sensor. All the Deimos-2 orthoimages were attained using the same medium resolution 10 m grid spacing DEM published by the Andalusian Government. Finally, the MS and PANSH orthoimages was also atmospherically corrected by using the ATCOR module, based on the MODTRAN (MODerate resolution atmospheric TRANsmission) radiative transfer code (Berk et al., 1998) implemented in Geomatica v. 2018.

It is important to note that, in the case of Deimos-2 imagery, four final orthoimages were generated: (i) orthoimage based on MS image with 4 m GSD and without atmospheric correction (Deimos-2 MS); (ii) orthoimage based on MS image with 4 m

GSD and atmospherically corrected by ATCOR (Deimos-2 MS ATCOR); (iii) orthoimage based on PANSH image with 1 m GSD and without atmospheric correction (Deimos-2 PANSH); (iv) orthoimage based on PANSH image with 1 m GSD and atmospherically corrected by ATCOR (Deimos-2 PANSH ATCOR).

2.4 Reference Greenhouses

The reference data consisted of 400 manually segmented objects located in the study area that were delineated over the WV3 PANSH RGB orthoimage with 0.3 m GSD (Fig. 2). This high number of reference polygons was recommended by Novelli et al. (2016) working on a work focused on mapping PCG. This number of reference geometries was also used by Aguilar et al. (2018). Both studies computed the modified ED2 metric using AssesSeg to evaluate the quality of the attained segmentations.

Figure 2. 400 reference geometries manually digitized (polygons in red) representing PCG on the WV3 PANSH RGB orthoimage.

3. METHODOLOGY

3.1 Image Segmentation

The image segmentation algorithm MRS included in the OBIA software Trimble eCognition Developer v. 9.5 (Trimble, Sunnyvale, CA, USA) was used in this work. This segmentation approach is a bottom-up region-merging technique starting with one-pixel objects. In numerous iterative steps, smaller objects are merged into larger ones (Baatz and Schäpe, 2000). The outcome of MRS algorithm is controlled by three main factors: (i) scale parameter (Scale), which determines the maximum heterogeneity allowed for the resulting segments, (ii) weight of colour and shape criteria in the segmentation process (Shape), and (iii) weight of the compactness and smoothness criteria (Compactness). The users also have to decide the bands combination and their corresponding weights to be applied in the segmentation process. Thousands of segmentations from applying MRS algorithm were computed over the four Deimos-2 orthoimages obtained by means of a semi-automatic eCognition rule set characterized by a looping process varying shape parameter (0.1 to 0.5 with a step of 0.1) and scale parameter (ranging from 40 to 1300), and setting compactness to 0.5 in all cases, according with the results provided by Aguilar et al. (2016a).

According to Novelli et al. (2017) the combination of bands for WV3 MS ATCOR orthoimage was set to equally weighted Blue-Green-NIR2 bands. On the other hand, the combination of bands for the four Deimos-2 orthoimages was always set to equally weighted Blue-Green-NIR bands.

3.2 Segmentation Quality Measures

Considering the goal of obtaining the best segmentation for each of the four orthoimages used in this work applying MRS, it is needed to use a method to measure the goodness of the segmentations performed through varying Scale and Shape parameters.

The Euclidean Distance 2 (ED2) discrepancy measure, originally proposed by Liu et al. (2012), provides both the geometrical discrepancy (potential segmentation error (PSE)) and the arithmetic discrepancy between image objects and reference polygons (number-of-segmentation ratio (NSR)). Between several supervised methods and metrics to quantitatively assess segmentation quality, Liu et al. (2012) recommended the ED2 measure. This metric also provided good results working on PCG (Aguilar et al., 2016a).

In this work, the selection of the best three MRS parameters for each image data was carried out through a modified version of ED2 including in a command line tool named AssesSeg. Full details about the modified ED2 measures as well as the standalone command line tool (AssesSeg.exe) is presented by Novelli et al. (2016). As a supervised segmentation quality metric, the modified ED2 works with a set of reference objects. In this work 400 reference greenhouses (Figure 2) were used. An optimal geometric match would be related to the absence of over-segmentation or under-segmentation. The best arithmetic match would occur when a reference polygon only matches a calculated object MRS. The best segmentation would be pointed out by the minimum value of modified ED2 measure, being zero the optimal combination of both geometric and arithmetic match.

4. RESULTS AND DISCUSSIONS

When the class to be segmented is very heterogeneous, as it is the case of PCG, between 200 and 300 manually digitized references should be considered to obtain reliable results (Aguilar et al., 2018). The optimal segmentations for each pre-processed orthoimage data from Deimos-2 (i.e., Deimos-2 MS, Deimos-2

MS ATCOR, Deimos-2 PANSH and Deimos-2 PANSH ATCOR) were attained using AssesSeg. The fixed parameters for all the four Deimos-2 orthoimages were the band combination (Blue-Green-NIR) and Compactness (0.5), while Shape and Scale parameters were kept variable. The selection of optimal segmentations were always based on the minimum value of the modified ED2 metric computed over the 400 polygons of reference (Figure 2).

Figure 3 depicts the values of modified ED2 computed for each segmentation extracted from Deimos-2 MS orthoimage. The red ellipse indicates the area where the best modified ED2 values were attained. In this case, the ED2 value was 0.455 by using a combination of 252, 0.5 and 0.5 values for Scale, Shape and Compactness parameters, respectively (Fig. 3). The Deimos-2 MS orthoimage presented the highest modified ED2 value (i.e., the worst results computed from MRS). The next worst segmentation turned out to be the one calculated on the Deimos-2 PANSH, being the ED2 value in this case of 0.418 by using a combination of 1242, 0.1 and 0.5 values for Scale, Shape and Compactness parameters, respectively (Fig. 4). The 1 m GSD of the Deimos-2 PANSH orthoimage managed to slightly improve the quality of optimal segmentation previously attained from 4 m GSD Deimos-2 MS. Again, the red ellipse shows the area with the best modified ED2 values, as in the following figures.

However, and according to Aguilar et al. (2018), what significantly improved the segmentation results from Deimos-2 data was the application of atmospheric corrections. In fact, when atmospheric corrections (ATCOR) were applied to the Deimos-2 MS orthoimage, the optimal ED2 value improved from 0.455 to 0.375 by using a combination a set of 55, 0.5 and 0.5 for Scale, Shape and Compactness parameters, respectively (Fig. 5).

Finally, the lowest value of modified ED2 (i.e., the best segmentation for Deimos-2) was computed on the MRS derived from the Deimos-2 PANSH ATCOR orthoimage. In this case, an ED2 value of 0.299 was attained by using a combination of 237, 0.4 and 0.5 values for Scale, Shape and Compactness parameters, respectively (Fig. 6).

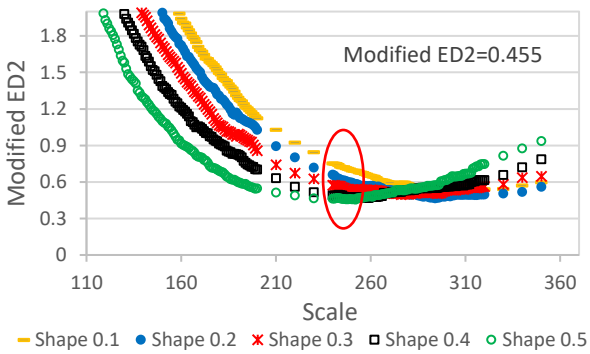

Figure 3. Modified ED2 computed by using AssesSeg for MRS outputs from Deimos-2 MS orthoimage.

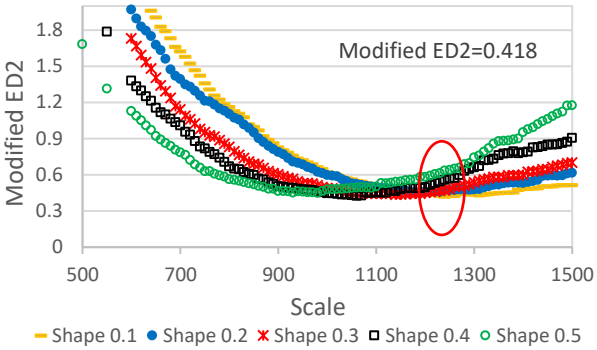

Figure 4. Modified ED2 computed by using AssesSeg for MRS outputs from Deimos-2 PANSH orthoimage.

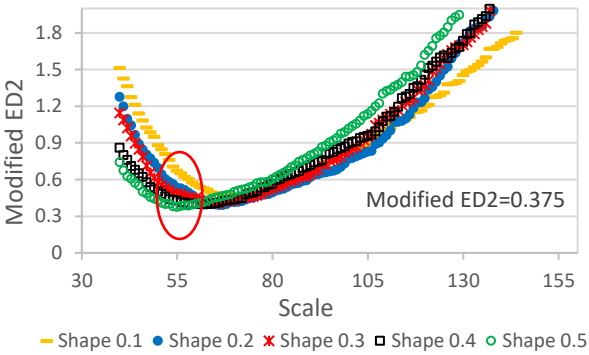

Figure 5. Modified ED2 computed by using AssesSeg for MRS outputs from Deimos-2 MS ATCOR orthoimage.

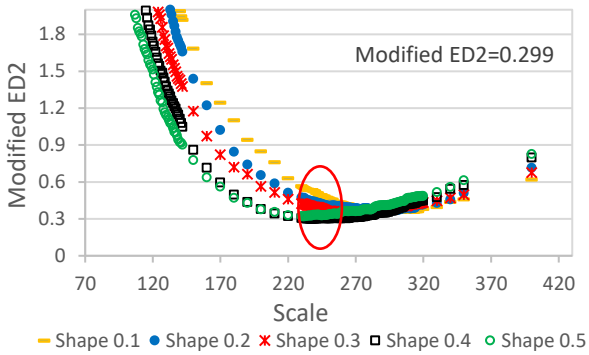

Figure 6. Modified ED2 computed by using AssesSeg for MRS outputs from Deimos-2 PANSH ATCOR orthoimage.

Aguilar et al. (2018) already reported that the application of atmospheric correction (ATCOR) in the VHR orthoimages resulted in a substantial reduction in the quantitative range of values or pixel relative mapping positions available for assigning pixel content (from 1 to 100% in the case of ground reflectance). This numerical effect, together with the mathematical formulation of the fusion factor or threshold employed for grouping pixels in the MRS algorithm, would imply that the higher the range of the pixel mapping content, the larger the number of objects would be segmented for a certain Scale parameter.

This contribution has been peer-reviewed. The double-blind peer-review was conducted on the basis of the full paper.
https://doi.org/10.5194/isprs-annals-V-2-2022-251-2022 | © Author(s) 2022. CC BY 4.0 License.

Figure 3, 4, 5 and 6 also show the importance of testing a wide range of parameters (mainly Scale and Shape) to find out the ideal segmentation based on each orthoimage. Notice that some tools previously developed to help user in setting these parameters, such as Estimation of Scale Parameters tool for a single band (ESP tool) (Drăgut et al., 2010) and for multiband images (ESP2 tool) (Drăgut et al., 2014), only search for the optimal scale parameter of MRS algorithm.

Figure 7 depicts a detailed view (area of around 1000 m per 1000 m) showing different optimal segmentations attained by using the 400 reference geometries and modified ED2. Figure 7a shows the reference geometries (400 red polygons), each one representing a single PCG. In the second row of Figure 7 the segmentations corresponding to Deimos-2 PANSH (without atmospheric correction) (Fig. 7b), and with ATCOR (Deimos-2 PANSH ATCOR) (Fig. 7c) are depicted in blue. In the third row, the segmentations derived from Deimos-2 MS orthoimages (i.e., Deimos-2 MS (Fig. 7d) and Deimos-2 MS ATCOR (Fig. 7e) are showed in light blue. It can be appreciated that the best segmentations, both visually and according to the modified ED2 values, were attained when ATCOR was applied. However, and applying a subjective visual analysis over the whole of greenhouses shown in Figure 7 (not only the reference geometries in red), the best segmentation seems to be depicted by Figure 7c (Deimos-2 PANSH ATCOR) closely followed by the results shown in Figure 7e (Deimos-2 MS ATCOR). Moreover, the segmentations presented in Figure 7b and 7d showed the highest discrepancy between segments (blue and light blue) and reference polygons (red). In all the cases, the modified ED2 presented a very good agreement with the visual quality of the greenhouse segmentations for all the studied cases.

Table 1 depicts the best MRS parameters according to the final values of modified ED2 obtained for each image source and Shape value. We can make out that regarding the best PCG segmentations, the Deimos-2 ATCOR PANSH orthoimage turned out to be the best image source with the lowest modified ED2 values. In this case, the ED2 values was ranging from 0.365 for Shape of 0.2, to 0.299 for a Shape value of 0.5. In addition, the optimal Shape parameter for each orthoimage was very variable. Because of that, the recommendations by Aguilar et al. (2016a) about selected a Shape parameter close to 0.3 should be taken carefully.

With the increasing of high-resolution satellite images, it is possible to recognize more detail on the Earth's surface. We analysed the segmentation quality in different pre-processed satellite images over PCG. In studies carried out previously, Aguilar et al. (2018) compared three VHR orthoimage from WV3 (WV3 MS, WV3, PAN and WV3 MS ATCOR), being the WV3 MS ATCOR corrected orthoimage the best image data source to attain the best PCG segmentation according to the modified ED2 metric.

In this paper, we evaluated the performance of four Deimos-2 derived datasets (Deimos-2 MS ATCOR, Deimos-2 MS, Deimos-2 PANSH ATCOR and Deimos-2 PANSH) on the segmentation outputs focused on PCG. The segmentation based on Deimos-2 PANSH ATCOR presented a good visual agreement with the real PCG land cover. Moreover, the modified ED2 metric attained for the optimal segmentation using Deimos-2 PANSH ATCOR orthoimage (ED2=0.299) was only slightly worse than the provided ones in previous works. For instance, Aguilar et al. (2018), working with a 1.2 m GSD WV3 MS ATCOR orthoimage taken on July 5, 2016, over almost the same study area but using 400 different reference geometries reported a minimum value of modified ED2 of 0.141, and it was yielded for a setting of 60, 0.4, 0.5, for Scale, Shape and Compactness, respectively. Novelli et al. (2016) working with the MRS algorithm applied to the 2 m GSD WV2 MS ATCOR orthoimage taken in July 2015 using the Blue-Green-NIR2 equally weighted band combination, reported a modified ED2 value of 0.198. In this case, the Scale, Shape, and Compactness parameters was set to 37, 0.4, and 0.5, respectively. In other work, Aguilar et al. (2016b) reported an optimal ED2 value of 0.290, for the same WV2 MS ATCOR orthoimage used by Novelli et al. (2016). However, in the last work, the band combination was composed of all eight equally weighted bands of WV2. In addition, the original ED2 metric proposed by Liu et al. (2012) was used instead of the modified ED2, and only 60 PCG were manually digitised as reference geometries. This time, the optimal MRS's parameters were 34, 0.3, and 0.5 for Scale, Shape, and Compactness, respectively.

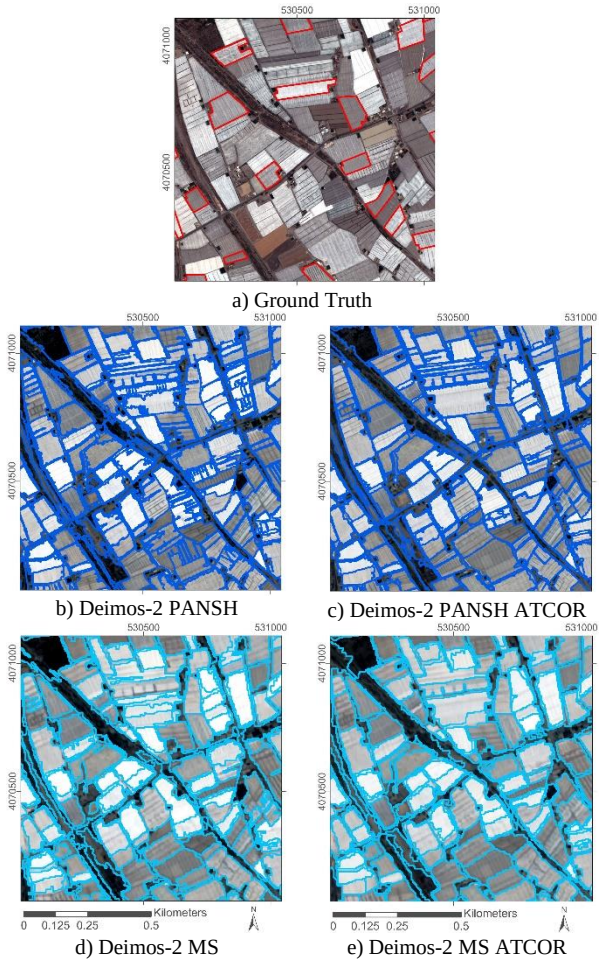

Figure 7. Visual comparison of the best achieved segmentations using MRS and AssesSeg over the corresponding RGB orthoimages: a) Reference geometries (400 red polygons) over WV3 MS ATCOR orthoimage; b) Optimal segmentation (Navy blue objects) derived from Deimos-2 PANSH orthoimage; c) Optimal segmentation (Navy blue objects) derived from Deimos-2 PANSH ATCOR orthoimage; d) Optimal segmentation (Clear blue objects) derived from Deimos-2 MS orthoimage; e) Optimal segmentation (Clear blue objects) derived from Deimos-2 MS ATCOR orthoimage. Coordinates in ETRS89 UTM Zone 30N.

This contribution has been peer-reviewed. The double-blind peer-review was conducted on the basis of the full paper.
https://doi.org/10.5194/isprs-annals-V-2-2022-251-2022 | © Author(s) 2022. CC BY 4.0 License.

Satellite	Ortho	Segmentation parameters			Modified ED2
		Scale	Shape	Compactness	
Deimos-2	MS (bands: Blue-Green-NIR)	309	0.1	0.5	0.538
		294	0.2	0.5	0.466
		276	0.3	0.5	0.496
		258	0.4	0.5	0.469
		252	0.5	0.5	**0.455**
Deimos-2	MS ATCOR (bands: Blue-Green-NIR)	71	0.1	0.5	0.464
		66	0.2	0.5	0.390
		65	0.3	0.5	0.403
		62	0.4	0.5	0.396
		55	0.5	0.5	**0.375**
Deimos-2	PANSH (bands: Blue-Green-NIR)	1242	0.1	0.5	**0.418**
		1192	0.2	0.5	0.445
		1158	0.3	0.5	0.433
		1058	0.4	0.5	0.424
		979	0.5	0.5	0.450
Deimos-2	PANSH ATCOR (bands: Blue-Green-NIR)	310	0.1	0.5	0.356
		296	0.2	0.5	0.365
		276	0.3	0.5	0.340
		237	0.4	0.5	**0.299**
		231	0.5	0.5	0.318

Table 1. Optimal MRS outputs (i.e., minimum ED2 values) for the different orthoimages tested and every Shape value.

5. CONCLUSIONS

More than 2800 segmentations on a PCG study site were generated in this study by using the well-known MRS algorithm included in eCognition. Four different pre-processed orthoimages from Deimos-2 satellite were used to attain the output segmentations.

Deimos-2 PANSH ATCOR orthoimage resulted to be the best tested image data source in order to attain an optimal PCG segmentation, according to both the modified ED2 metric and visual interpretation. This orthoimage product presented a GSD of 1 m and digital values expressed as ground reflectance. Moreover, the segmentations selected using the modified ED2 metric presented a very good visual agreement with the real PCG land cover.

The PCG optimal segmentations derived from Deimos-2 MS orthoimages with 4 m GSD, both with and without atmospheric corrections, achieved quite worse results. Furthermore, Deimos-2 PANSH with 1 m GSD but without atmospheric corrections, also presented a quite poor segmentation.

The application of atmospheric corrections significantly improved the segmentation results from Deimos-2 data. It seems that the substantial reduction in the quantitative range of digital values when atmospheric corrections are applied improve the PCG segmentations. This fact will required further investigations.

It was very important to test a wide range of parameters to find out the ideal segmentation based on each orthoimage. In this sense, the command line tool AssesSeg allowed easily checking a high number of MRS parameters combinations.

With the forthcoming rapid development of the PCG areas over the world, future works will focus on evaluate new segmentation algorithms and metrics for quantifying segmentation quality.

ACKNOWLEDGEMENTS

This research was funded by Spanish Ministry for Science, Innovation and Universities (Spain) and the European Union (European Regional Development Fund, ERDF) funds, grant number RTI2018-095403-B-I00 This study takes part in the general research lines promoted by the Agrifood Campus of International Excellence ceiA3.

REFERENCES

Aguilar, M.A., Saldaña, M.M., Aguilar, F.J., 2013. GeoEye-1 and WorldView-2 Pan-Sharpened Imagery for Object-Based Classification in Urban Environments. *International Journal of Remote Sensing*, 34(7), 2583-2606. doi.org/10.1080/01431161.2012.747018.

Aguilar, M.A., Bianconi, F., Aguilar, F.J., Fernández, I., 2014. Object-Based Greenhouse Classification from GeoEye-1 and WorldView-2 Stereo Imagery. *Remote Sensing* 6(5), 3554-3582. doi.org/10.3390/rs6053554.

Aguilar, M., Aguilar, F., García Lorca, A., Guirado, E., Betlej, M., Cichon, P., Nemmaoui, A., Vallario, A., Parente, C., 2016a. Assessment of multiresolution segmentation for extracting greenhouses from WorldView-2 imagery. *Int. Arch. Photogramm. Remote Sens. Spatial Inf. Sci*., XLI-B7, 145-152.

Aguilar, M.A., Nemmaoui, A., Novelli, A., Aguilar, F.J., García Lorca, A., 2016b. Object-Based Greenhouse Mapping Using Very High Resolution Satellite Data and Landsat 8 Time Series. *Remote Sensing*, 8, 513. doi:10.3390/rs8060513.

Aguilar, M.A., Novelli, A., Nemamoui, A., Aguilar, F.J., García-Lorca, A.M., González-Yebra, Ó., 2018. Optimizing Multiresolution Segmentation for Extracting Plastic Greenhouses from Worldview-3 Imagery. In: De Pietro G., Gallo L., Howlett R., Jain L. (eds) Intelligent Interactive Multimedia Systems and Services 2017. KES-IIMSS-18 2018. Smart Innovation, Systems and Technologies, vol 76. Springer, Cham. doi.org/10.1007/978-3-319-59480-4_4.

Aguilar, M.A., Jiménez-Lao, R., Nemmaoui, A., Aguilar, F.J., 2020. Geometric Accuracy Assessment of Deimos-2 Panchromatic Stereo Pairs: Sensor Orientation and Digital Surface Model Production. *Sensors*, 20(24), 7234. doi.org/10.3390/s20247234.

Baatz, M, Schäpe, M., 2000. Multiresolution Segmentation - An Optimization Approach for High Quality Multi-Scale Image Segmentation Angewandte Geographische Informationsverarbeitung XII. In: Strobl, J., Blaschke, T., Griesebner, G. (Eds.), Angewandte Geographische Informations-Verarbeitung XII. Wichmann Verlag, Karlsruhe, pp. 12-23.

Blaschke, T., Hay, G.J., Kelly, M., Lang, S., Hofmann, P., Addink, E., Feitosa, R.Q., van der Meer, F., van der Werff, H., van Coillie, F., Tiede, D., 2014. Geographic Object-Based Image Analysis—Towards a new paradigm. *ISPRS Journal Photogrammetry and Remote Sensing*, 87(2014), 180-191. doi.org/10.1016/j.isprsjprs.2013.09.014.

Berk, A., Bernstein, L.S., Anderson, G.P., Acharya, P.K., Robertson, D.C., Chetwynd, J.H., Adler-Golden, S.M., 1998. MODTRAN Cloud and Multiple Scattering Upgrades with Application to AVIRIS. *Remote Sensing of Environment*, 65, 367–375. doi.org/10.1016/S0034-4257(98)00045-5

Carleer, A.P., Wolff, E., 2006. Urban land cover multi-level region-based classification of VHR data by selecting relevant features. *International Journal of Remote Sensing*, 27(6), 1035-1051. doi.org/10.1080/01431160500297956.

Drăgut, L., Tiede, D., Levick, S., 2010. ESP: a tool to estimate scale parameters for multiresolution image segmentation of remotely sensed data. *International Journal of Geographical Information Science*, 24(6), 859-871.

Drăgut, L., Csillik, O., Eisank, C., Tiede, D., 2014. Automated parameterisation for multi-scale image segmentation on multiple layers. *ISPRS Journal Photogrammetry and Remote Sensing*, 88(2014), 119-127.

Fernández, I., Aguilar, F.J., Aguilar, M.A., Álvarez, M.F., 2014. Influence of Data Source and Training Size on Impervious Surface Areas Classification Using VHR Satellite and Aerial Imagery through an Object-Based Approach. *IEEE Journal of Selected Topics in Applied Earth Observations and Remote Sensing*, 7(12), 4681-4691. doi.org/10.1109/JSTARS.2014.2327159.

Heenkenda, M.K., Joyce, K.E., Maier, S.W., 2015. Mangrove Tree Crown Delineation from High-Resolution Imagery. *Photogrammetric Engineering and Remote Sensing*, 81(6), 471-479. doi.org/10.14358/PERS.81.6.471.

Hossain, M.D., Chen, D., 2019. Segmentation for Object-Based Image Analysis (OBIA): A Review of Algorithms and Challenges from Remote Sensing Perspective. *ISPRS Journal of Photogrammetry and Remote Sensing*, 150, 115-134. doi.org/10.1016/j.isprsjprs.2019.02.009.

Jiménez-Lao, R., Aguilar, F.J., Nemmaoui, A., Aguilar, M.A., 2020. Remote Sensing of Agricultural Greenhouses and Plastic-Mulched Farmland: An Analysis of Worldwide Research. *Remote Sensing*, 12(16), 2649. doi.org/10.3390/RS12162649.

Johnson, B.A., Ma, L., 2020. Image Segmentation and Object-Based Image Analysis for Environmental Monitoring: Recent Areas of Interest, Researchers' Views on the Future Priorities. *Remote Sensing*, 12, 1772. doi.org/10.1016/j.isprsjprs.2020.01.002.

Jozdani S., Chen, D., 2020. On the versatility of popular and recently proposed supervised evaluation metrics for segmentation quality of remotely sensed images: An experimental case study of building extraction. *ISPRS Journal of Photogrammetry and Remote Sensing*, 160, 275-290. doi.org/10.1016/J.ISPRSJPRS.2012.01.007.

Kotaridis, I., Lazaridou, M., 2021. Remote Sensing Image Segmentation Advances: A Meta-Analysis. *ISPRS Journal of Photogrammetry and Remote Sensing*, 173, 309-322. doi.org/10.1016/j.isprsjprs.2021.01.020.

Liu, Y., Bian, L., Meng, Y., Wang, H., Zhang, S., Yang, Y., Shao, X., Wang, B., 2012. Discrepancy Measures for Selecting Optimal Combination of Parameter Values in Object-Based Image Analysis. *ISPRS Journal of Photogrammetry and Remote Sensing*, 68, 144–156. doi.org/10.1016/J.ISPRSJPRS.2012.01.007.

Marpu, P.R., Neubert, M., Herold, H., Niemeyer, I., 2010. Enhanced Evaluation of Image Segmentation Results. *Journal of Spatial Science*, 55(1), 55-68. doi.org/10.1080/14498596.2010.487850.

Mesner, N., Oštir, K., 2014. Investigating the Impact of Spatial and Spectral Resolution of Satellite Images on Segmentation Quality. *Journal of Applied Remote Sensing*, 8(1), 083696. doi.org/10.1117/1.jrs.8.083696.

Novelli, A., Aguilar, M.A., Nemmaoui, A., Aguilar, F.J., Tarantino, E., 2016. Performance Evaluation of Object Based Greenhouse Detection from Sentinel-2 MSI and Landsat 8 OLI Data: A Case Study from Almería (Spain). *International Journal of Applied Earth Observation and Geoinformation*, 52, 403-11. doi.org/10.1016/j.jag.2016.07.011.

Novelli, A., Aguilar, M.A., Aguilar, F,J,m Nemmaoui, A., Tarantino, E., 2017. AssesSeg—A Command Line Tool to Quantify Image Segmentation Quality: A Test Carried Out in Southern Spain from Satellite Imagery. *Remote Sensing*, 9(1), 40. doi.org/10.3390/rs9010040.

Pacifici, F, Longbotham, N., Emery, W.J., 2014. The Importance of Physical Quantities for the Analysis of Multitemporal and Multiangular Optical Very High Spatial Resolution Images. *IEEE Transactions on Geoscience and Remote Sensing*, 52(10), 6241-6256. doi.org/10.1109/TGRS.2013.2295819.

Petrushevsky, N., Manzoni, M., Monti-Guarnieri, A., 2022. Fast Urban Land Cover Mapping Exploiting Sentinel-1 and Sentinel-2 Data. *Remote Sensing*, 14 (1), 36. doi.org/10.3390/rs14010036.

Pu, R., Landry, S., Yu, Q., 2011. Object-based urban detailed land cover classification with high spatial resolution IKONOS imagery. *International Journal of Remote Sensing*, 32(12), 3285-3308. doi.org/10.1080/01431161003745657.

Pu, R., Landry, S., 2012. A comparative analysis of high spatial resolution IKONOS and WorldView-2 imagery for mapping urban tree species. *Remote Sensing of Environment*, 124(2012), 516-533. doi.org/10.1016/j.rse.2012.06.011.

Stumpf, A., Kerle, N., 2011. Object-oriented mapping of landslides using Random Forests. *Remote Sensing of Environment*, 115(2011), 2564-2577. doi.org/10.1016/j.rse.2011.05.013.

Tarantino, E., Figorito, B., 2012. Mapping rural areas with widespread plastic covered vineyards using true color aerial data. *Remote Sensing*, 4, 1913-1928. doi.org/10.3390/rs4071913.

Tetteh, G.O., Gocht, A., Erasmi, S., Schwieder, M., Conrad, C., 2021, Evaluation of Sentinel-1 and Sentinel-2 Feature Sets for Delineating Agricultural Fields in Heterogeneous Landscapes.

IEEE Access, 9, 116702-116719. doi.org/10.1109/ACCESS.2021.3105903.

Witharana, C., Civco, D.L., 2014. Optimizing multi-resolution segmentation scale using empirical methods: exploring the sensitivity of the supervised discrepancy measure Euclidean distance 2 (ED2). *ISPRS Journal Photogrammetry and Remote Sensing*, 87(2014), 108-121. doi.org/10.1016/j.isprsjprs.2013.11.006.

Zhang, H., Fritts, J.E., Goldman, S.A., 2008. Image Segmentation Evaluation: A Survey of Unsupervised Methods. *Computer Vision and Image Understanding*, 110(2), 260-280. doi.org/10.1016/j.cviu.2007.08.003.